

Cells stably expressing shRNA against MYO10 display altered cell motility

Joanna A. Mas^{1*}, Chase E. Cristella^{1*}, Vu Hao M.N. Phan^{1*}, Lillian S. Wendt¹, Charlotte A. Rose¹, Abigail Ali¹, David F. Carpio¹, Christine Cole¹, Paige Embley¹, Jack E. Hoskins-Harris¹, Delia Johnson¹, Noelle Ledoux¹, Hannah W. Lwin¹, Sarah Salah¹, Erin Weisbart², Stacey J. Criswell¹, Omar Alberto Quintero-Carmona^{1§}

¹Department of Biology, University of Richmond, Richmond, Virginia, United States

²Imaging Platform, Broad Institute, Cambridge, Massachusetts, United States

§To whom correspondence should be addressed: oquinter@richmond.edu

*These authors contributed equally.

Abstract

Myosin-X (MYO10) is an actin-based motor protein involved in cytoskeletal dynamics, membrane interactions, and integrin-mediated adhesion. To investigate MYO10's cellular roles, we generated MYO10 knockdown (MYO10^{KD}) HeLa and COS7 cell lines using lentiviral shRNA. Compared to wild-type cells, both MYO10^{KD} lines showed reduced proliferation and impaired cell migration in wound assays. Additionally, there were fewer edge filopodia in HeLa cells. Furthermore, MYO10^{KD} cells demonstrated increased spreading on laminin-coated substrates, suggesting altered integrin activation and cytoskeletal linkage. Our results reinforce MYO10's importance in cell proliferation, adhesion, and migration. These MYO10^{KD} lines provide an accessible cell culture model for future study of MYO10.

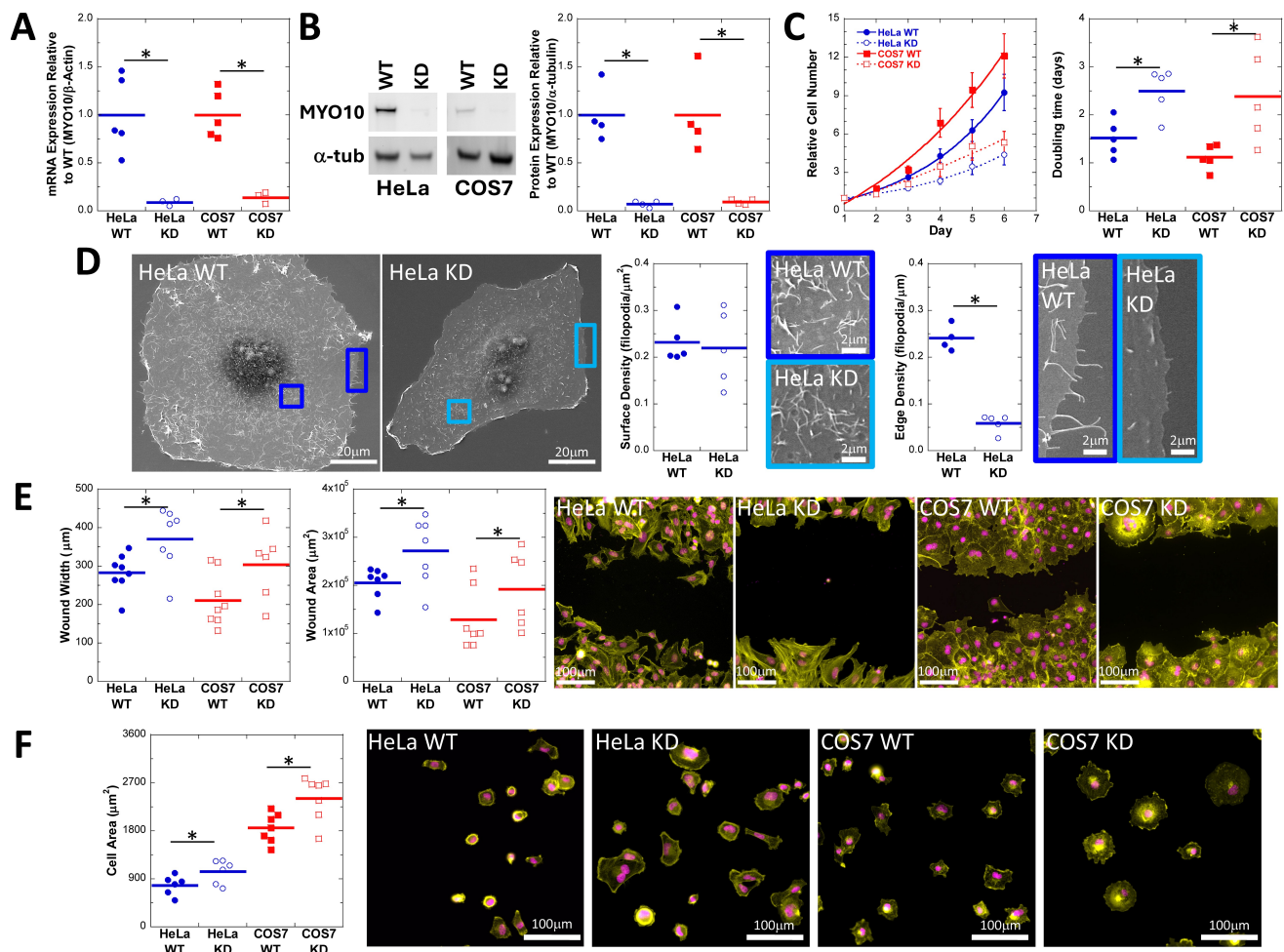


Figure 1. Decreased MYO10 expression in two different cell lines stably expressing shRNA results in proliferation, motility, and attachment defects compared to wild-type parental cell lines:

Semi-clonal HeLa and COS7 lines isolated by puromycin selection show decreased MYO10 mRNA and protein expression as measured by (A) qPCR or (B) quantitative western blotting. The MYO10 band is nearly undetectable in a

representative western blot. Blots against α -tubulin were used as a standard for quantification. **(C)** Both HeLa and COS7 MYO10^{KD} cells proliferate more slowly than their parental lines. The curve is a fit to a single exponential growth, and slower proliferation was quantified as the increased doubling-time for the shRNA expressing cells. **(D)** MYO10^{KD} HeLa cells maintain the ability to form dorsal surface filopodia with no change in filopodial density, but do show decreased edge filopodia density. The colored boxes on the lower magnification images correspond to the borders of the higher magnification images. **(E)** Cell migration following wounding is impaired in MYO10^{KD} cells, as demonstrated by decreased wound width or wound area 18h after monolayer wounding. **(F)** Cell spreading on laminin-coated surfaces is enhanced in MYO10^{KD} cell lines, as illustrated by increased cell area 2 hours after initial plating. *Quantitative and statistical representations:* For all plots, circle and square markers represent biological replicates, horizontal bars represent the mean across replicates, and asterisks represent Student's t-test with $p < 0.05$. For the growth curve plot in (C), markers represent the average of biological replicates and traces represent fitting the averaged data to single exponential growth. Representative images in (E) and (F) are stained for actin (ALEXA488-phalloidin, yellow) and DNA (DAPI, magenta).

Description

In eukaryotic cells, both cell migration and the organization of internal components rely on a cytoskeletal system composed of filaments, motor proteins, and their associated regulators (reviewed in Machesky and Schliwa, 2000). The class X myosin proteins (MYO10) play roles in both cytoskeletal dynamics and membrane interactions (Kerber and Cheney, 2011; Tokuo, 2020). MYO10 facilitates the formation of filopodia (Berg and Cheney, 2002; Bohil et al., 2006; Tokuo et al., 2007), promotes directed migration (Arjonen et al., 2011; Hwang et al., 2009), and links actin filaments to membrane-bound receptors such as integrins (Cox et al., 2002; He et al., 2017; Toyoshima and Nishida, 2007; Zhang et al., 2004). Given these roles, MYO10 is thought to contribute to spatially coordinated signaling events essential for cell proliferation, adhesion, and motility. To better understand the mechanistic contributions of MYO10 in these contexts, we generated and characterized MYO10 knockdown cell lines using lentiviral delivery of short hairpin RNA (shRNA) resulting in genomic integration (Dull et al., 1998). By doing so, we aimed to generate an accessible cell culture model system for investigating the roles of MYO10 in cytoskeletal organization, migratory capacity, and adhesive behavior. These cell lines also provide a useful platform for studying the functionality of specific MYO10 domains and sequences through ectopic expression of fluorescently tagged or mutant constructs.

Cell culture model systems are more useful for studying the behavior of fluorescently tagged proteins-of-interest if the endogenous expression of that protein is reduced. By minimizing the confounding behavior of the native protein, observed phenotypes can be attributed to the exogenously expressed protein. Although embryonic fibroblasts isolated from MYO10 knockout mice (MYO10^{KO} MEFs) are available (Heimsath et al., 2017; Yim et al., 2023), we were unable to achieve robust transient transfection in MYO10^{KO} MEFs using the lipid-based methodology available to us. Commonly available mammalian cell culture models such as HeLa cells (Scherer et al., 1953), a human cervical carcinoma line, and COS7 cells (Gluzman, 1981), an African green monkey kidney epithelia line, are easily transfectable and have been used extensively to study MYO10 function (Berg and Cheney, 2002; Bishai et al., 2013; Kerber et al., 2009; Raines et al., 2012; Tokuo and Ikebe, 2004). These cell lines are also amenable to lentiviral delivery of shRNA-containing plasmids, which result in low-frequency genomic incorporation of lentiviral DNA. If the delivered plasmid also contains a puromycin mammalian antibiotic resistance marker, then semi-clonal lines can be identified when cultured in the presence of the antibiotic. Antibiotic-resistant sub-cultures can then be screened for decreased MYO10 mRNA and protein expression (Moffat et al., 2006). Verification of knockdown was done via qPCR analysis of MYO10 mRNA levels (Figure 1A) and quantitative western blot analysis of MYO10 protein levels (Figure 1B). Relative mRNA expression was reduced by >80% in shRNA-expressing HeLa (wildtype = 1.0 ± 0.2 , knockdown = 0.09 ± 0.02) and COS7 (wildtype = 1.0 ± 0.1 , knockdown = 0.14 ± 0.04) cell lines (MYO10^{KD}) compared to their wild-type parental lines (Student's t-test, HeLa $p < 0.006$, COS7 $p < 0.0009$). Relative protein expression was reduced by >90% in HeLa (wildtype = 1.0 ± 0.1 , knockdown = 0.07 ± 0.02) and COS7 (wildtype = 1.0 ± 0.2 , knockdown = 0.09 ± 0.01) MYO10^{KD} cell lines compared to their MYO10^{WT} parental lines (Student's t-test, HeLa $p < 0.008$, COS7 $p < 0.02$).

We assayed the HeLa and COS7 MYO10^{KD} cell lines for their growth characteristics (Figure 1C). When doubling time was calculated from fitting growth data to single exponential growth, the observed doubling time was significantly slower for MYO10^{KD} lines. Doubling time increased in HeLa (wildtype = 1.5 ± 0.2 days, knockdown = 2.5 ± 0.2 days) and COS7 (wildtype = 1.1 ± 0.1 days, knockdown = 2.4 ± 0.4 days) MYO10^{KD} lines compared to their MYO10^{WT} parental lines (Student's t-test, HeLa $p < 0.008$, COS7 $p < 0.04$). MYO10 regulates both mitotic and meiotic spindle positioning, indicating a central role in cell division. In mammalian culture cells, MYO10 contributes to planar spindle orientation required for proper centromere and spindle orientation (Toyoshima and Nishida, 2007) and alignment with cell geometry (Kwon et al., 2015). In *Xenopus* models, MYO10 disruption leads to spindle positioning defects in meiotic spindles (Weber et al., 2004); in mitotic spindles MYO10 disruption results in elongated spindles and an increase in the fraction of cells with multipolar spindles, possibly due to increased spindle fragmentation (Woolner et al., 2008). MYO10 also interacts with

components of the cell division machinery including microtubules (Weber et al., 2004) and TPX2 (Woolner et al., 2008). Interactions between MYO10 and WEE1 impact phoshoCDK1 localization and anaphase onset in epithelial cell cultures (Sandquist et al., 2018). In addition to direct involvement in spindle dynamics and function, upregulation of MYO10 is often a feature of tumors, and MYO10 depletion leads to decreased tumor growth in animal models (Mayca Pozo et al., 2023; Mayca Pozo et al., 2021). The slowed-growth pattern that we observed in MYO10^{KD} cells is consistent with other findings where expression changes in MYO10 led to changes in cellular processes central to cell proliferation.

HeLa cells generate filopodia on their dorsal surfaces and along their edges, while COS7 cells do not generate dorsal filopodia and have very few edge filopodia (Berg and Cheney, 2002; Bohil et al., 2006). Previous reports described differences in filopodia formation following transient siRNA treatment to reduce MYO10 expression (Bohil et al., 2006). We used scanning electron microscopy to assay HeLa MYO10^{KD} cells for their ability to generate dorsal and edge filopodia (Figure 1D). We observed a significant decrease in the density of filopodia along the periphery of HeLa MYO10KD (0.06±0.01 filopodia/μm) when compared to HeLa MYO10WT cells (0.24±0.01 filopodia/μm, Student's t-test, p<0.0001). However, analysis of dorsal surfaces showed no difference in filopodial densities between HeLa MYO10^{KD} and HeLa MYO10^{WT} cells, which differs from previous reports (Bohil et al., 2006; Pi et al., 2007). It is possible that the acute loss of MYO10 by transient siRNA transfection leads to different behavior than cells stably expressing shRNA, as cells stably expressing shRNA may have upregulated compensatory pathways that lead to dorsal filopodia formation (El-Brolosy and Stainier, 2017). It is also possible that the HeLa cell lines used in this study are potentially quite different from the HeLa cells used previously. There is a growing literature demonstrating that different HeLa cell isolates have different genomic signatures which could result in differences in phenotypes and behaviors (Fratini et al., 2015; Hu et al., 2019; Landry et al., 2013; Liu et al., 2019).

We used a wound-healing assay (Liang et al., 2007) to examine the effect of MYO10 knockdown on collective cell migration. Briefly, cells were grown to near-confluency on coverslips, the monolayer was disrupted by gentle scratching with a pipet tip, and the wounds were fixed and examined following 18 hours of recovery in low-serum media to limit the impact of cell division on wound closure. Recovery was measured by either quantifying the width of the wound, or by assaying the area of the wound visible in each image (Figure 1E). Wound width increased in HeLa (wildtype = 283±18μm, knockdown = 370±31μm) and COS7 (wildtype = 211±24μm, knockdown = 304±36μm) MYO10^{KD} lines compared to their MYO10^{WT} parental lines (paired Student's t-test, HeLa p<0.006, COS7 p<0.02). Wound area increased in HeLa (wildtype = 2.1±0.1x10⁵ μm², knockdown = 2.7±0.3x10⁵ μm²) and COS7 (wildtype = 1.3±0.2x10⁵ μm², knockdown = 1.9±0.3x10⁵ μm²) MYO10^{KD} lines compared to their MYO10^{WT} parental lines (paired Student's t-test, HeLa p<0.01, COS7 p<0.03). Both MYO10^{KD} cell lines migrated into the wound more slowly than their MYO10^{WT} counterparts as illustrated by wider wound widths and by larger wound areas. Our results are consistent with previous findings showing a reduction in cell motility following MYO10 knockdown as represented by decreases in cell migration across multiple cell types with reduced MYO10 expression (Makowska et al., 2015; Tokuo et al., 2018; Yu et al., 2015). These differences in behavior could be due to changes in filopodial assembly dynamics or to differences in the cells' ability to adhere to substrates due to decreased MYO10 function. MYO10's role in interacting with the extracellular matrix to form adhesions and influence motility makes it an integral component of the cell's migratory machinery (He et al., 2017; Yu et al., 2015; Zhang et al., 2004). Knocking down MYO10 greatly reduces the interactions between the cell and the extracellular matrix, potentially making it more difficult for cells to move.

MYO10 serves as a link between the actin cytoskeleton and extracellular matrix proteins through integrin-mediated adhesions (Alieva et al., 2019; Zhang et al., 2004). Laminin is one such extracellular matrix protein. We used cell spreading assays on laminin-coated surfaces to evaluate the impact of decreased MYO10 expression on integrin-mediated attachment for both HeLa and COS7 cells. MYO10^{KD} and MYO10^{WT} cells were allowed to adhere to laminin-coated coverslips for 2 hours prior to fixation and phalloidin staining. The cells were then imaged and their attachment area was quantified (Figure 1F) using Ilastik (Berg et al., 2019) to identify cell area. Cell area was larger in HeLa (wildtype = 781±75 μm², knockdown = 1036±91μm²) and COS7 (wildtype = 1857±105 μm², knockdown = 2415±155 μm²) MYO10^{KD} lines compared to their MYO10^{WT} parental lines (paired Student's t-test, HeLa p<0.05, COS7 p<0.02). Previous studies have also reported similar increases in cell spreading with decreased MYO10 expression (Bohil et al., 2006). Integrin activation and adhesion may be functioning as a governor, slowing the speed of cellular protrusion through the connection to the cytoskeleton via MYO10 (Courson and Cheney, 2015; Watanabe et al., 2010). MYO10 knockdown has been shown to impair integrin activation at filopodia tips, even though integrins remain localized along the filopodia shaft (Miihkinen et al., 2021). This impaired spatial regulation of integrin activity and decreased linkage between the integrins and the cytoskeleton may disrupt normal responses to the extracellular matrix, contributing to the enhanced spreading phenotype observed here. Our findings are consistent with the two-step model proposed by Miihkinen et al., where MYO10 tethers integrins at filopodia tips to facilitate talin-mediated activation (Miihkinen et al., 2021). MYO10 depletion would thus dysregulate this process, altering adhesion dynamics and spreading behavior (Yu et al., 2015).

Taken together, the phenotypes of these HeLa and COS7 MYO10^{KD} cells align with other previous reports of MYO10 knockdown (Bohil et al., 2006; Makowska et al., 2015), and knockout cell phenotypes (Heimsath et al., 2017; Ou et al., 2022; Tokuo et al., 2018). These new cell lines will aid in the study of MYO10 as they can be easily transfected with fluorescently tagged and modified versions of MYO10, allowing any scientist with cell culture and fluorescence imaging capabilities to investigate how particular changes to wild-type MYO10 structure influences MYO10. As lentiviral shRNA delivery systems are available for much of the mouse and human genome (Moffat et al., 2006), generation and characterization of knockdown cell lines could provide other undergraduate scientists with an opportunity for authentic contribution to broader scientific understanding for other genes, just as this project has for University of Richmond students gaining experience in quantitative imaging approaches for studying cell function.

Methods

COS7 and HeLa cell culture

Cos7 (Gluzman, 1981) and HeLa (Scherer et al., 1953) cells were cultured in growth media: DMEM high glucose (Gibco) supplemented with 10% Fetal Bovine Serum (Benchmark FBS, GeminiBio), and antibiotics (50U/ml penicillin, 50mg/ml streptomycin, Gibco). Cells were maintained in a humidified incubator at 37°C with 5% CO₂ concentration and passaged using 0.25% trypsin-EDTA (Gibco).

Lentivirus and stable cell line production

HEK293FT cells (a gift from Benjamin Major, UNC Chapel Hill) were grown in growth media. The cells were maintained at 37°C in a humidified environment supplemented with 5% CO₂. To generate virus, Lipofectamine 3000 (Invitrogen) was used as the transfection reagent, and cells grown in T75 plates pCMV-VSV-G (Stewart et al., 2003), pRSV-Rev, pMDLg/pRRE (Dull et al., 1998) (Addgene plasmid # 8454, 12253, and 12251, respectively), pLKO.1 plasmid TRCN0000123087 (Moffat et al., 2006) targeting the human MYO10 sequence (target sequence: CCCAGATGAGAAGATATTCAA, Millipore Sigma), and a small amount of pEGFP-C1 to verify transfection. Twenty four hours later, media containing the virus was collected and replaced with fresh media. Cellular debris was removed from the virus-containing media by centrifugation at 2000 x g for 5 minutes at 4°C prior to infection.

HeLa cells and COS7 cells were plated in T25 flasks and grown to confluency. They were then incubated with lentivirus media diluted into DMEM growth at a 1:4 or a 4:1 viral media:growth media ratio. The media was supplemented with 8mg/ml hexadimethrine bromide and the infected plates were incubated overnight. The following day, the cells in the T25 were transferred to 150mm cell culture dishes and grown in media containing 2μg/ml puromycin. Media was replaced every two days to remove debris from dying cells. The plates were examined for clusters of isolated cells assumed to be colonies of cells where the DNA containing the shRNA cassette and the puromycin resistance gene had been incorporated into the cells' genome. Eight to ten days after infection, clusters were isolated by placing a cloning ring in sterile petroleum jelly surrounding a colony. The colony was trypsinized, transferred to one well of a 6-well dish, and cultured in puromycin-containing growth media. The cultures were grown and expanded for 10 more days prior to verification of MYO10 knockdown by qPCR and western blotting. At this point, validated cultures of HeLa cells and COS7 cells were designated "passage #1," and aliquots were frozen in DMEM growth media supplemented with 10% cell culture-grade DMSO (Sigma) and 40% fetal bovine serum.

Quantitative Real Time PCR sample preparation and analysis

RNA was isolated from T25-sized cultures of HeLa or COS7 cells using the RNeasy Plus kit (Qiagen) according the supplied protocol for purification of RNA from animal cells. In addition to the standard protocol, we also treated the cells to a Qias shredder step before loading the cell lysate onto the purification column, and we treated the lysate with an on-column DNase digestion prior to washing and eluting the RNA. RNA concentration was estimated using a Nanodrop spectrophotometer, aliquoted, and frozen at -80°C.

cDNA was synthesized using the M-MLV reverse transcriptase kit with random hexamer primers, following the standard protocol, with a starting amount of 750μg RNA (Invitrogen). qPCR samples were prepared using the Luna Universal qPCR Master Mix (New England Biolabs) and run on a Bio-Rad CFX96 real time PCR machine, and assayed for MYO10 expression and β-actin expression. Standard curves for both MYO10 and β-actin were generated and run in parallel with the cell line cDNA samples—all samples in triplicate. MYO10 expression relative to β-actin expression was quantified using Bio-Rad CFX Manager software and was standardized relative to the wild-type cell MYO10/β-actin ratio for the relevant knockdown line.

Western blotting

Cells were lysed in sample buffer containing protease inhibitors (50 mM Tris HCl, pH 7.4, 0.5 M NaCl, 0.2% SDS, 1 mM EDTA, 1 mM DTT, 10 mg/ml aprotinin, 10 mg/ml leupeptin, 1 mM PMSF) at a concentration of 2x10⁶ cells/ml. After adding an appropriate volume of 5x Lamelli sample buffer, the samples were heated to 95°C for 5 minutes, and then allowed to cool to room temperature. Samples were loaded onto a 4-12% Bis-Tris NuPAGE gel, and run at ~180V until

the dye front reached the bottom of the gel. Proteins were transferred to Immuno-Blot Low Fluorescence PVDF Membrane, using an XCell II blotting apparatus (Invitrogen) in NuPAGE transfer buffer with 20% methanol for 60 minutes at 30V. Transfer was verified by Ponceau staining (0.5% Ponceau Red-S in 2% Acetic acid). Membranes were incubated in blocking buffer (1% Casein in TBS) for 1 hour prior to incubation with rabbit α -MYO10 antibody (Abcam #ab224120, 1 μ g/mL in blocking buffer) overnight at 4°C with gentle agitation. The blots were then washed 4 times in TBST for 10 minutes, and then incubated with hFAB™ Rhodamine α -tubulin (part#12004166 and 1:5000) and donkey α -rabbit ALEXA647 antibody (Jackson ImmunoResearch, 0.15 μ g/mL in blocking buffer) for 1 hour. Blots were washed 4 times in TBST for 10 minutes each prior to visualization using a Bio-Rad ChemiDoc MP system using the CY5 and Rhodamine filter sets to visualize MYO10 and tubulin staining, respectively.

Western blotting quantification and analysis

Band intensities were quantified using the “Analyze Gels” tool in FIJI/ImageJ (Schindelin et al., 2012). The MYO10/tubulin ratio was calculated for each sample, where the average MYO10/tubulin ratio for the wild-type cells was set to a value of 1, and all other MYO10/tubulin ratios were standardized relative to this value.

Growth curve sample preparation, data acquisition, and analysis

The cell proliferation assay protocol was adapted from (Rago et al., 1990). Cells were plated in six 96-well cell culture plates at a density of 1000 cells/well in 100 μ L of growth media and incubated in a humidified environment at 37°C with 5% CO₂. Empty wells were filled with 100 μ L of sterile water to prevent media evaporation. Sufficient plates were set up at the beginning of the experiment so that one plate could be collected each day of the experiment. Each day, one plate was removed from the incubator, and media was discarded by gently shaking the plate over a sink, followed by blotting on a paper towel. The plate was then stored at -80°C. This process was repeated at the same time for subsequent days. All plates were kept at -80°C for an additional 24 hours following the final time day. Plates were thawed at room temperature for approximately an hour. After thawing, 100 μ L of sterile water was added to each well. To induce lysis, plates were incubated at 37°C for one hour before being returned to -80°C overnight. Plates were removed from -80°C, thawed at room temperature for an hour, and stained with 100 μ L of staining buffer (10mM Tris, 2M NaCl, 1mM EDTA, 2mM NaN₃, 2.5mg/mL Hoescht 33342, pH 7.4). Plates were incubated at room temperature in the dark for 30 minutes before fluorescence measurement. Fluorescence intensity was recorded using a Spectramax M3 plate reader (Molecular Devices) with the following settings: excitation/emission range of 360-460 nm, no shaking, and a top-down detection mode (plate lids removed prior to reading). Data was saved and exported as Excel files for further analysis.

Raw absorbance data was pasted into a spreadsheet for analysis. Background absorbance values were determined using sterile water wells and subtracted from all sample wells. To calculate fold-growth, absorbance values for each condition were normalized to the average absorbance on Day 1. Average fold growth values across multiple experiments were plotted using KaleidaGraph software, and were then fit to a single exponential growth model. The exponential growth curve was used to determine the doubling time at Day 4.

SEM sample preparation, imaging, and filopodial density quantification

Before processing, a 6-well dish was prepared, where wild-type or MYO10 knockdown HeLa cells were plated on acid-washed, 18 mm round #1.5 coverslips at a concentration of 25,000 cells/well in growth media, and allowed to adhere overnight. The following day, media was removed, and samples were fixed in warm PBS containing 4% paraformaldehyde and 2% glutaraldehyde for at least 30 minutes with gentle rocking. Fixative was removed with three, 10-minute PBS washes. Samples were dehydrated via a series of ethanol washes at 30%, 50%, 70%, 95%, and 100% ethanol for 10 mins at each concentration. Samples were submerged in 100% ethanol and critical-point dried using a Samdri-795. After drying, samples were mounted on 12.2 mm diameter, 10 mm high aluminum mounts and sputter-coated with a Leica EM ACE600 ~10nm of 60/40 gold/palladium to prevent the buildup of surface charges. Samples were then imaged using a JEOL JSM-IT700HR scanning electron microscope set to a working distance of 15mm, a standard probe current (STD-PC) of 50, and a field of view of 128 μ m \times 96 μ m.

To reduce the potential for bias, SEM images were randomized using a “Blind Experiment” plugin in FIJI-ImageJ. Randomized images were then opened in FIJI. To calculate dorsal filopodia density, a region of interest (ROI) was highlighted using the “Rectangle” tool for each cell present in the image. The ROI was then enlarged, and dorsal filopodia were manually counted using the “Cell Counter” plugin. Filopodial surface density (filopodia/mm²) was then calculated through the counted filopodia by the area of the region of interest. To calculate edge density, the length of free cell edge was measured and the number of filopodia along that edge were counted (filopodia/mm).

Wound healing assay sample preparation & imaging

On day 1, both HeLa and COS7 wild-type and MYO10 knockdown cells were plated on square glass coverslips at a concentration of 120,000 cells per well in growth media and allowed to adhere overnight. On day 2, once confluency was verified, cells were scratched. Using a P10 pipette tip, the coverslip upon which the cells were growing on was scratched 5 total times. 3 of the scratches were done in parallel vertically, and 2 of the scratches were done in parallel horizontally.

This allowed up to 5 possible “lanes” of observation when image capturing. After scratching, the media from these wells was removed, and 3 mLs of Low-Serum Media was added to prevent cellular division. Wounds were allowed to heal for 18 hours, after which cells were then permeabilized in PBS with 0.5% Triton X100 for 5 minutes. Samples were stained for F-actin and DNA with 6.6nM ALEXA488-phalloidin and 15nM DAPI for 30 minutes. After four 5-minute PBS washes, the cells were mounted onto slides using Profade Glass. Images were captured using an Olympus UPlanSApo20x/0.75NA objective mounted on either an IX-71 or IX-83 stand, an EXFO mixed gas light source, a Chroma Sedat Quad filter set, and a Hamamatsu ORCA Flash 4v2 camera. The microscopy hardware and image acquisition settings were controlled by Metamorph software. Typical exposure times were under 30ms for DAPI and under 150ms for ALEXA488-phalloidin.

Wound healing assay quantification, widths

Using the straight line tool in FIJI/ImageJ, ten lines were traced from one side of the wound to the other, approximately perpendicular to the wound edge for each image. Line lengths were recorded in pixels, converted to microns, and averaged for each day. A minimum of 10 images were captured for each sample condition on each day.

Wound healing assay quantification, area

Wound area was completed using both Ilastik (Berg et al., 2019) and FIJI/ImageJ. With Ilastik, the images captured on the channel visualizing F-actin were uploaded to the application. “Cell” and “background” pixels were identified using the “Pixel Classification” segmentation workflow, with all options selected in the “Feature Selection” step. The classifier was trained using 15-20% of the total number of pictures in a set. Scratches from each day, cell type, and condition were trained individually. Simple segmentations were exported as TIF files. The resulting segmented files were thresholded in FIJI/ImageJ, the wound areas were measured for each image, and averaged together for each condition on each day. A minimum of 10 images were captured for each condition on each day.

Spreading assay sample preparation & imaging

Prior to plating, acid-washed, 22mm square #1.5 coverslips were placed in a 6 well dish, coated with 10μg/mL laminin in PBS for 30 minutes, and then washed 3x with PBS. Cells were lifted using 0.25% trypsin with EDTA, and then resuspended at a concentration of 20,000 cells/mL in DMEM supplemented with 10% fetal bovine serum, penicillin, and streptomycin. 3 mL of the cell mixture were added to each well for a total of 60,000 cells/well, and allowed to adhere for the specified amount of time. Once the time-course ended, the media was removed and the cells were fixed in PBS with 4% paraformaldehyde for 20 minutes. Cells were then permeabilized in PBS with 0.5% Triton X100 for 5 minutes. Samples were stained for F-actin and DNA with 6.6nM ALEXA568-phalloidin and 15nM DAPI for 30 minutes. After four 5-minute PBS washes, the cells were mounted onto slides using Profade Glass. Images were captured using an Olympus UPlanSApo20x/0.75NA objective mounted on either an IX-71 or IX-83 stand, an EXFO mixed gas light source, a Chroma Sedat Quad filter set, and a Hamamatsu ORCA Flash 4v2 camera. The microscopy hardware and image acquisition settings were controlled by Metamorph software. Typical exposure times were under 30ms for DAPI and under 150ms for ALEXA568-phalloidin.

Spreading assay quantification, area

Measurement of cell area was completed using both Ilastik and FIJI/ImageJ. With Ilastik, the images captured on the channel visualizing F-actin were uploaded to the application. “Cell” and “background” pixels were identified using the “Pixel Classification” segmentation workflow, with all options selected in the “Feature Selection” step. The classifier was trained using 15-20% of the total number of pictures in a set. Samples from each day, cell type, and condition were trained individually. Simple segmentations were exported as TIF files. The resulting segmented files were thresholded in FIJI/ImageJ, cell areas were measured for each image, and averaged together for each condition on each day. A minimum of 10 images were captured for each condition on each day.

Replication and statistical analysis

For qPCR, each marker represents the average of 2-3 technical replicates for a particular experiment (n = 3 or 4 experiments). For western blotting, each marker represents a single sample for a particular experiment (n = 4 experiments). For growth curves and doubling time calculations, each marker represents the average of 5-7 different experiments where each experiment contained triplicate technical replicates. For dorsal filopodia density, each marker represents the average of >15 measured cells (n = 5 experiments). For wound width, each marker represents the average of >50 width measurements across multiple wounds (n = 6, 7, or 8 experiments). For wound area, each marker represents the average of >10 different images of wounds (n = 6 or 7 experiments). For spreading area, each marker represents the average of >90 cells (n = 6 or 7 experiments). Statistical comparisons between conditions within a cell type (wild-type versus knockdown) were carried out using a Student’s t-test. Data are reported in the text as mean ± standard error of the mean. As wounding width variation is sensitive to the experimenter carrying out the scratch, wound data was compared using a paired Student’s t-test.

Acknowledgements: The results in this report were generated primarily by undergraduate students working in the Quintero lab and the Spring BIOL317 Mechanochemical Cell Biology Course at the University of Richmond. OAQ-C

generated the lentivirus and established the cell lines, CEC validated the cell lines using qPCR and western blotting, JAM completed the growth assays, VMNP completed the scanning electron microscopy analysis, and CEC & JAM collaborated on the scratch analysis. Once the cell lines were established the students in BIOL317 used the lines as part of a course-based undergraduate research experience where they became proficient at collecting fluorescence microscopy data, and basic segmentation and quantitative image analysis under the guidance of SJC, EW, and OAQ-C. JAM was the BIOL317 teaching assistant responsible for cell line maintenance and sample preparation. The students chose to analyze cell spreading and other measures of size & shape. Validation of the results came from multiple teams of students using different instruments to collect and analyze images from the same sets of slides. The students then compared results across all teams within the class. To get exposure and immersion to the cell science field, the students presented their results in a “Zoom lab meeting” at the end of the semester to Hijab Fatima (Columbia University), Jordan Beach (Loyola University Chicago), Richard Cheney (UNC Chapel Hill), Tom Pollard (Yale University), Derek Applewhite (Reed College), Meg Titus (University of Minnesota), Kendall Stewart (UC Davis), Gabe Offenback (UNC Chapel Hill), Graham Johnson (Allen Institute for Cell Science), Uri Manor (UC San Diego), Sarah Heissler (The Ohio State University), Adelaide Masterson (Latham BioPharm Group), Anthony Isenhour (Yale University), Dan Kiehart (Duke University), and John Peters (Harvard University). The BIOL317 team would like to thank these scientists for their time, their support, and their insight. Their participation was crucial to giving the students a sense that their efforts have value to the greater cell science community. We thank the University of Richmond School of Arts & Sciences for establishing and maintaining the [Biological Imaging Lab](#). Laboratory courses based in modern microscopy approaches are uncommon at the undergraduate level and prepare Richmond students for future success in science.

Part of this work can be found on bioRxiv (Mas et al., 2025).

References

- Alieva NO, Efremov AK, Hu S, Oh D, Chen Z, Natarajan M, et al., Bershadsky AD. 2019. Myosin IIA and formin dependent mechanosensitivity of filopodia adhesion. *Nat Commun.* 10: 3593. 38. PubMed ID: [31399564](#)
- Arjonen A, Kaukonen R, Ivaska J. 2011. Filopodia and adhesion in cancer cell motility. *Cell Adh Migr.* 5: 421-30. 7. PubMed ID: [21975551](#)
- Berg JS, Cheney RE. 2002. Myosin-X is an unconventional myosin that undergoes intrafilopodial motility. *Nat Cell Biol.* 4: 246-50. 4. PubMed ID: [11854753](#)
- Berg S, Kutra D, Kroeger T, Straehle CN, Kausler BX, Haubold C, et al., Kreshuk A. 2019. ilastik: interactive machine learning for (bio)image analysis. *Nat Methods.* 16: 1226-1232. 39. PubMed ID: [31570887](#)
- Bishai EA, Sidhu GS, Li W, Dhillon J, Bohil AB, Cheney RE, Hartwig JH, Southwick FS. 2013. Myosin-X facilitates Shigella-induced membrane protrusions and cell-to-cell spread. *Cell Microbiol.* 15: 353-367. 20. PubMed ID: [23083060](#)
- Bohil AB, Robertson BW, Cheney RE. 2006. Myosin-X is a molecular motor that functions in filopodia formation. *Proc Natl Acad Sci U S A.* 103: 12411-6. 5. PubMed ID: [16894163](#)
- Courson DS, Cheney RE. 2015. Myosin-X and disease. *Exp Cell Res.* 334: 10-5. 41. PubMed ID: [25819274](#)
- Cox D, Berg JS, Cammer M, Chingwundoh JO, Dale BM, Cheney RE, Greenberg S. 2002. Myosin X is a downstream effector of PI(3)K during phagocytosis. *Nat Cell Biol.* 4: 469-77. 12. PubMed ID: [12055636](#)
- Dull T, Zufferey R, Kelly M, Mandel RJ, Nguyen M, Trono D, Naldini L. 1998. A third-generation lentivirus vector with a conditional packaging system. *J Virol.* 72: 8463-71. 13. PubMed ID: [9765382](#)
- El Brolosy MA, Stainier DYR. 2017. Genetic compensation: A phenomenon in search of mechanisms. *PLoS Genet.* 13: e1006780. 29. PubMed ID: [28704371](#)
- Frattini A, Fabbri M, Valli R, De Paoli E, Montalbano G, Gribaldo L, Pasquali F, Maserati E. 2015. High variability of genomic instability and gene expression profiling in different HeLa clones. *Sci Rep.* 5: 15377. 30. PubMed ID: [26483214](#)
- Gluzman Y. 1981. SV40-transformed simian cells support the replication of early SV40 mutants. *Cell.* 23: 175-82. 17. PubMed ID: [6260373](#)
- He K, Sakai T, Tsukasaki Y, Watanabe TM, Ikebe M. 2017. Myosin X is recruited to nascent focal adhesions at the leading edge and induces multi-cycle filopodial elongation. *Sci Rep.* 7: 13685. 10. PubMed ID: [29057977](#)
- Heimsath EG, Yim YI, Mustapha M, Hammer JA, Cheney RE. 2017. Myosin-X knockout is semi-lethal and demonstrates that myosin-X functions in neural tube closure, pigmentation, hyaloid vasculature regression, and filopodia formation. *Sci Rep.* 7: 17354. 14. PubMed ID: [29229982](#)
- Hu WE, Zhang X, Guo QF, Yang JW, Yang Y, Wei SC, Su XD. 2019. HeLa-CCL2 cell heterogeneity studied by single-cell DNA and RNA sequencing. *PLoS One.* 14: e0225466. 33. PubMed ID: [31790455](#)

- Hwang YS, Luo T, Xu Y, Sargent TD. 2009. Myosin-X is required for cranial neural crest cell migration in *Xenopus laevis*. *Dev Dyn*. 238: 2522-9. 8. PubMed ID: [19718754](#)
- Kerber ML, Cheney RE. 2011. Myosin-X: a MyTH-FERM myosin at the tips of filopodia. *J Cell Sci*. 124: 3733-41. 3. PubMed ID: [22124140](#)
- Kerber ML, Jacobs DT, Campagnola L, Dunn BD, Yin T, Sousa AD, Quintero OA, Cheney RE. 2009. A novel form of motility in filopodia revealed by imaging myosin-X at the single-molecule level. *Curr Biol*. 19: 967-73. 18. PubMed ID: [19398338](#)
- Kwon M, Bagonis M, Danuser G, Pellman D. 2015. Direct Microtubule-Binding by Myosin-10 Orients Centrosomes toward Retraction Fibers and Subcortical Actin Clouds. *Dev Cell*. 34: 323-37. 23. PubMed ID: [26235048](#)
- Landry JJ, Pyl PT, Rausch T, Zichner T, Tekkedil MM, Stutz AM, et al., Steinmetz LM. 2013. The genomic and transcriptomic landscape of a HeLa cell line. G3 (Bethesda). 3: 1213-24. 32. PubMed ID: [23550136](#)
- Liang CC, Park AY, Guan JL. 2007. In vitro scratch assay: a convenient and inexpensive method for analysis of cell migration in vitro. *Nat Protoc*. 2: 329-33. 34. PubMed ID: [17406593](#)
- Liu Y, Mi Y, Mueller T, Kreibich S, Williams EG, Van Drogen A, et al., Aebersold R. 2019. Multi-omic measurements of heterogeneity in HeLa cells across laboratories. *Nat Biotechnol*. 37: 314-322. 31. PubMed ID: [30778230](#)
- Machesky LM, Schliwa M. 2000. Cell dynamics: a new look at the cytoskeleton. *Nat Cell Biol*. 2: E17-8. 1. PubMed ID: [10620818](#)
- Makowska KA, Hughes RE, White KJ, Wells CM, Peckham M. 2015. Specific Myosins Control Actin Organization, Cell Morphology, and Migration in Prostate Cancer Cells. *Cell Rep*. 13: 2118-25. 36. PubMed ID: [26670045](#)
- Mas JA, Cristella CE, Phan VMN, Wendt LS, Rose CA, Ali A, et al., Quintero-Carmona. 2025. Cells stably expressing shRNA against MYO10 display altered cell motility. : 10.1101/2025.07.23.666455. DOI: [10.1101/2025.07.23.666455](#)
- Mayca Pozo F, Geng X, Miyagi M, Amin AL, Huang AY, Zhang Y. 2023. MYO10 regulates genome stability and cancer inflammation through mediating mitosis. *Cell Rep*. 42: 112531. 27. PubMed ID: [37200188](#)
- Mayca Pozo F, Geng X, Tamagno I, Jackson MW, Heimsath EG, Hammer JA, Cheney RE, Zhang Y. 2021. MYO10 drives genomic instability and inflammation in cancer. *Sci Adv*. 7: eabg6908. 26. PubMed ID: [34524844](#)
- Miihkinen M, Gronloh MLB, Popovic A, Vihinen H, Jokitalo E, Goult BT, Ivaska J, Jacquemet G. 2021. Myosin-X and talin modulate integrin activity at filopodia tips. *Cell Rep*. 36: 109716. 42. PubMed ID: [34525374](#)
- Moffat J, Grueneberg DA, Yang X, Kim SY, Kloepfer AM, Hinkle G, et al., Root DE. 2006. A lentiviral RNAi library for human and mouse genes applied to an arrayed viral high-content screen. *Cell*. 124: 1283-98. 22. PubMed ID: [16564017](#)
- Ou H, Wang L, Xi Z, Shen H, Jiang Y, Zhou F, Liu Y, Zhou Y. 2022. MYO10 contributes to the malignant phenotypes of colorectal cancer via RACK1 by activating integrin/Src/FAK signaling. *Cancer Sci*. 113: 3838-3851. 43. PubMed ID: [35912545](#)
- Pi X, Ren R, Kelley R, Zhang C, Moser M, Bohil AB, et al., Patterson C. 2007. Sequential roles for myosin-X in BMP6-dependent filopodial extension, migration, and activation of BMP receptors. *J Cell Biol*. 179: 1569-82. 28. PubMed ID: [18158328](#)
- Rago R, Mitchen J, Wilding G. 1990. DNA fluorometric assay in 96-well tissue culture plates using Hoechst 33258 after cell lysis by freezing in distilled water. *Anal Biochem*. 191: 31-4. 46. PubMed ID: [1706565](#)
- Raines AN, Nagdas S, Kerber ML, Cheney RE. 2012. Headless Myo10 is a negative regulator of full-length Myo10 and inhibits axon outgrowth in cortical neurons. *J Biol Chem*. 287: 24873-83. 21. PubMed ID: [22661706](#)
- Sandquist JC, Larson ME, Woolner S, Ding Z, Bement WM. 2018. An interaction between myosin-10 and the cell cycle regulator Wee1 links spindle dynamics to mitotic progression in epithelia. *J Cell Biol* 217(3): 849-859. PubMed ID: [29321170](#)
- Scherer WF, Syverton JT, Gey GO. 1953. Studies on the propagation in vitro of poliomyelitis viruses. IV. Viral multiplication in a stable strain of human malignant epithelial cells (strain HeLa) derived from an epidermoid carcinoma of the cervix. *J Exp Med*. 97: 695-710. 16. PubMed ID: [13052828](#)
- Schindelin J, Arganda Carreras I, Frise E, Kaynig V, Longair M, Pietzsch T, et al., Cardona A. 2012. Fiji: an open-source platform for biological-image analysis. *Nat Methods*. 9: 676-82. 45. PubMed ID: [22743772](#)
- Stewart SA, Dykxhoorn DM, Palliser D, Mizuno H, Yu EY, An DS, et al., Novina CD. 2003. Lentivirus-delivered stable gene silencing by RNAi in primary cells. *RNA*. 9: 493-501. 44. PubMed ID: [12649500](#)
- Tokuo H. 2020. Myosin X. *Adv Exp Med Biol*. 1239: 391-403. 2. PubMed ID: [32451868](#)

Tokuo H, Bhawan J, Coluccio LM. 2018. Myosin X is required for efficient melanoblast migration and melanoma initiation and metastasis. *Sci Rep.* 8: 10449. 35. PubMed ID: [29993000](#)

Tokuo H, Ikebe M. 2004. Myosin X transports Mena/VASP to the tip of filopodia. *Biochem Biophys Res Commun.* 319: 214-20. 19. PubMed ID: [15158464](#)

Tokuo H, Mabuchi K, Ikebe M. 2007. The motor activity of myosin-X promotes actin fiber convergence at the cell periphery to initiate filopodia formation. *J Cell Biol.* 179: 229-38. 6. PubMed ID: [17954606](#)

Toyoshima F, Nishida E. 2007. Integrin-mediated adhesion orients the spindle parallel to the substratum in an EB1- and myosin X-dependent manner. *EMBO J.* 26: 1487-98. 11. PubMed ID: [17318179](#)

Watanabe TM, Tokuo H, Gonda K, Higuchi H, Ikebe M. 2010. Myosin-X induces filopodia by multiple elongation mechanism. *J Biol Chem.* 285: 19605-14. 40. PubMed ID: [20392702](#)

Weber KL, Sokac AM, Berg JS, Cheney RE, Bement WM. 2004. A microtubule-binding myosin required for nuclear anchoring and spindle assembly. *Nature.* 431: 325-9. 24. PubMed ID: [15372037](#)

Woolner S, O'Brien LL, Wiese C, Bement WM. 2008. Myosin-10 and actin filaments are essential for mitotic spindle function. *J Cell Biol.* 182: 77-88. 25. PubMed ID: [18606852](#)

Yim YI, Pedrosa A, Wu X, Chinthalapudi K, Cheney RE, Hammer JA. 2023. Myosin 10 uses its MyTH4 and FERM domains differentially to support two aspects of spindle pole biology required for mitotic spindle bipolarity. *bioRxiv* 15. PubMed ID: [37398378](#)

Yu H, Lai M, Guo Y, Yuan L, Lan Y, Wang X, Zhu X. 2015. Myo10 is required for neurogenic cell adhesion and migration. *In Vitro Cell Dev Biol Anim.* 51: 400-7. 37. PubMed ID: [25491426](#)

Zhang H, Berg JS, Li Z, Wang Y, Lang P, Sousa AD, et al., Stromblad S. 2004. Myosin-X provides a motor-based link between integrins and the cytoskeleton. *Nat Cell Biol.* 6: 523-31. 9. PubMed ID: [15156152](#)

Funding: The University of Richmond School of Arts & Sciences funded undergraduate summer research for JAM, CEC, VMNP, and LSW through "[The Richmond Guarantee](#)." The University of Richmond Department of Biology funded academic-year independent research for CEC and VMNP, as well as the undergraduate research component of BIOL317. This work was supported by the CBEC: Path to Publication grant, NSF RCN:UBE award no. 2316122.

Author Contributions: Joanna A. Mas: data curation, formal analysis, investigation, methodology, supervision, validation, visualization, writing - original draft, writing - review editing. Chase E. Cristella: data curation, formal analysis, investigation, methodology, validation, visualization, writing - original draft, writing - review editing. Vu Hao M.N. Phan: data curation, formal analysis, investigation, methodology, visualization, writing - original draft, writing - review editing. Lillian S. Wendt: data curation, formal analysis, investigation, visualization, writing - original draft, writing - review editing. Charlotte A. Rose: data curation, formal analysis, investigation, methodology, visualization, writing - original draft, writing - review editing. Abigail Ali: data curation, formal analysis, investigation, methodology, visualization. David F. Carpio: data curation, formal analysis, investigation, methodology, visualization. Christine Cole: data curation, formal analysis, investigation, methodology, visualization. Paige Embley: data curation, formal analysis, investigation, methodology, visualization. Jack E. Hoskins-Harris: data curation, formal analysis, investigation, methodology, visualization. Delia Johnson: data curation, formal analysis, investigation, methodology, visualization. Noelle Ledoux: data curation, formal analysis, investigation, methodology, visualization. Hannah W. Lwin: data curation, formal analysis, investigation, methodology, visualization. Sarah Salah: data curation, formal analysis, investigation, methodology, visualization. Erin Weisbart: formal analysis, methodology, supervision, writing - review editing. Stacey J. Criswell: conceptualization, funding acquisition, methodology, project administration, resources, supervision, writing - review editing. Omar Alberto Quintero-Carmona: conceptualization, data curation, formal analysis, funding acquisition, investigation, methodology, project administration, resources, supervision, validation, visualization, writing - original draft, writing - review editing.

Reviewed By: Anonymous

History: Received July 24, 2025 **Revision Received** September 3, 2025 **Accepted** September 17, 2025 **Published Online** September 19, 2025

Copyright: © 2025 by the authors. This is an open-access article distributed under the terms of the Creative Commons Attribution 4.0 International (CC BY 4.0) License, which permits unrestricted use, distribution, and reproduction in any medium, provided the original author and source are credited.

Citation: Mas JA, Cristella CE, Phan VHMN, Wendt LS, Rose CA, Ali A, et al., Quintero-Carmona OA. 2025. Cells stably expressing shRNA against MYO10 display altered cell motility. *microPublication Biology.* [10.17912/micropub.biology.001764](#)